J Mol Model (2011) 17:181–200
DOI 10.1007/s00894-010-0712-x

ORIGINAL PAPER

Conformational analysis of piperazine and piperidine analogs of GBR 12909: stochastic approach to evaluating the effects of force fields and solvent

Deepangi Pandit · William Roosma · Milind Misra · Kathleen M. Gilbert · William J. Skawinski · Carol A. Venanzi

Received: 7 February 2010 / Accepted: 16 March 2010 / Published online: 23 April 2010

Abstract Analogs of the flexible dopamine reuptake inhibitor, GBR 12909 (**1**), may have potential utility in the treatment of cocaine abuse. As a first step in the 3D-QSAR modeling of the dopamine transporter (DAT)/serotonin transporter (SERT) selectivity of these compounds, we carried out conformational analyses of two analogs of **1**: a piperazine (**2**) and a related piperidine (**3**). Ensembles of conformers consisting of local minima on the potential energy surface of the molecule were generated in the vacuum phase and in implicit solvent by random search conformational analysis using the Tripos and MMFF94 force fields. Some differences were noted in the conformer populations due to differences in the treatment of the tertiary amine nitrogen and ether oxygen atom types by the force fields. The force fields also differed in their descriptions of internal rotation around the C(sp^3)–O(sp^3) bond proximal to the bisphenyl moiety. Molecular orbital calculations at the HF/6-31G(d) and B3LYP/6-31G(d) levels of C–O internal rotation in model compound (**5**), designed to model the effect of the proximity of the bisphenyl group on C-O internal rotation, showed a broad region of low energy between −60° to 60° with minima at both −60° and 30° and a low rotational barrier at 0°, in closer agreement with the MMFF94 results than the Tripos results. Molecular mechanics calculations on model compound (**6**) showed that the MMFF94 force field was much more sensitive than the Tripos force field to the effects of the bisphenyl moiety on C–O internal rotation.

Keywords Conformational analysis · GBR 12909 · Dopamine reuptake inhibitor · Dopamine transport · Molecular mechanics · Stochastic search · Conformer population · Molecular orbital · Tripos force field · MMFF94 force field

Electronic supplementary material The online version of this article (doi:10.1007/s00894-010-0712-x) contains supplementary material, which is available to authorized users.

D. Pandit · M. Misra · K. M. Gilbert · W. J. Skawinski · C. A. Venanzi (✉)
Department of Chemistry and Environmental Science,
New Jersey Institute of Technology,
323 King Blvd.,
Newark, NJ 07102-1982, USA
e-mail: venanzi@adm.njit.edu

W. Roosma
Department of Computer Science,
New Jersey Institute of Technology,
323 King Blvd.,
Newark, NJ 07102-1982, USA

Present Address:
D. Pandit
BioMaPS Institute for Quantitative Biology, Rutgers,
the State University of New Jersey,
610 Taylor Road,
Piscataway, NJ 08854-8087, USA

Present Address:
M. Misra
Multiscale Dynamic Materials Modeling Department,
Sandia National Laboratories,
Albuquerque, NM 87185-1413, USA

Introduction

The "dopamine hypothesis" [1] implicates the dopamine transporter (DAT) in cocaine abuse and addiction. A DAT-selective dopamine reuptake inhibitor, which could prevent cocaine from binding to the DAT yet allow some reuptake of dopamine through the DAT without having cocaine's addictive effects, would be useful in pharmacoptherapy for

cocaine abuse. Structure–activity relationship (SAR) studies for a class of dopamine reuptake inhibitor based on the GBR 12909 scaffold have been reviewed [2, 3], and have provided a basis for three-dimensional quantitative structure–activity relationship (3D-QSAR) computer modeling studies [4, 5]. GBR 12909, 1-[2-[bis(4-fluorophenyl) methoxy]ethyl]-4-(3-phenylpropyl) piperazine, **1** (Fig. 1), is the parent compound of the analogs used in the present study. Dutta et al. [6] showed that only one of the two nitrogens in the central ring system was required for activity at the dopamine transporter. However, the SAR of the piperidine analogs appears to be somewhat different from that of the piperazines [2, 7–11].

Since such flexible molecules may adopt a wide range of closely related conformations, one way to begin to investigate differences in the piperazine and piperadine analogs at the molecular level is to examine the conformer populations of two such analogs. This approach, first suggested by Boyd and Coner [12], has the advantage of allowing one to compare a full range of conformers found within a certain energy window, rather than just a single structure of each analog. Here we study two GBR 12909 analogs that differ only in their central ring systems. Analogs **2** [13] (a piperazine; Fig. 1) and **3** [9] (a piperidine; Fig. 1) were chosen because they are somewhat less flexible than **1** and are therefore easier to treat computationally. They have fewer rotatable bonds than **1** on the A- (or napthyl) side of the molecule, while the B- (or bisphenyl) side is exactly the same as **1**. Analog **3** has the highest DAT binding affinity and the largest degree of DAT/SERT (serotonin transporter) selectivity of the three compounds (Table 1).

Since the GBR 12909 analogs are much more flexible than other dopamine reuptake inhibitors such as methylphenidate (**4**, Fig. 1), it is possible that the structures and relative energies of their conformers could be influenced to some degree by the force field and solvation model used in the calculation. To investigate this possibility, we compare conformer populations of **2** and **3** obtained through random search conformational analysis using the Tripos force field [14] and the Merck Molecular Force Field 94 (MMFF94) [15–21]. Although the MMFF94 force field has been extensively compared to other force fields in terms of conformational energies and intermolecular interaction energies and geometries [21], the Tripos force field was not included in that study because it was developed and validated [14] for use without charges, and so was considered by the author to be unsuitable for the description of intermolecular interactions. The performance of the Tripos force field (without charges) has been compared to an earlier version of the Merck Molecular Force Field, MMFF93, by Gundertofte et al. [22], who recommended that the Tripos force field should be validated for each class of compounds to which it is to be applied. Using the same data set of 44 compounds as used in the MMFF93 study, a recent comparison of the Tripos and MMFF94 force fields concluded that MMFF94 gives superior results for conformational energy differences and rotational barriers [23].

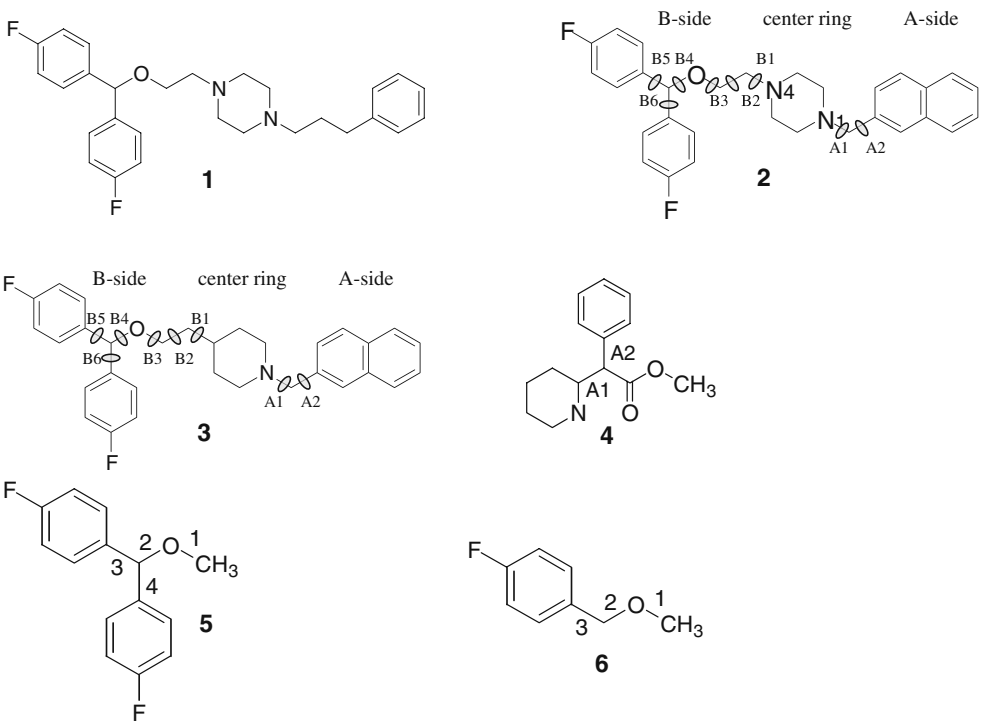

Fig. 1 Structures of GBR 12909, **1**; its analogs **2** and **3**; methylphenidate, **4**; and the model compounds 1,1′-(methoxymethylene)bis(4-fluorobenzene), **5**, and 1-fluoro-4-(methoxymethyl)benzene, **6**. Torsion angles used in the study are labeled A1, A2, B1, ..., B6 (and are indicated by *elliptical shapes*) for **2** and **3**, A1 and A2 for **4**, 1–4 for **5**, and 1–3 for **6**

Table 1 Binding affinities[a] at the DAT and SERT

Analog	DAT K_i	SERT K_i	SERT/DAT ratio
1, GBR 12909[b]	3.7 (± 0.4)	126 (±27)	34
2[c]	8.0 (±0.3)	312 (±15)	39
3[b]	0.72 (±0.06)	229 (±21)	323

[a] K_i is given in nanomoles (nM), standard deviations are shown in parentheses

[b] Reference [9]

[c] Reference [13]

The present work follows the recommendation of Gundertofte et al. by investigating the treatment of representative analogs of the GBR 12909 class of dopamine reuptake inhibitors by the MMFF94 and Tripos force fields.

The above force field comparison studies were carried out on small molecules. It is possible that certain large functional groups (such as the bisphenyl moiety) in the GBR 12909 analogs could affect the rotational barriers around nearby bonds (such as C–O). For that reason, we carried out molecular mechanics and molecular orbital calculations on model compounds in order to investigate the effect of the bisphenyl group on C–O internal rotation.

The SYBYL software package (available from Tripos, Inc., St. Louis, MO, USA) offers both the MMFF94 and Tripos force field options, as well as a variety of atomic charge set options for use with the Tripos force field. There are many examples in the literature in which the Tripos force field is used with a particular atomic charge set without any justification or validation. For this reason, we felt that a comparison of the results of conformational analysis with the MMFF94 force field (and associated MMFF94 charges) to those obtained with the Tripos force field (and Gasteiger–Hückel charges) would be useful. Since the SYBYL package also offers a simple solvent model (a distance-dependent dielectric function), we included this model in the study in order to see the "gross" effects of solvent on conformational populations. The study is not meant to be an extensive study of solvation effects.

Since the piperazine and piperidine moieties of **2** and **3** are common to many pharmaceutically important compounds, an in-depth examination of their treatment in these two different force fields is particularly relevant. For example, the conformer populations of **2** and **3** generated with the Tripos vacuum-phase force field and analyzed here were used by us in a 3D-QSAR modeling study of the DAT/SERT selectivity of 48 piperazine and piperidine GBR 12909 analogs with changes on the A-side only [5]. In addition, the conformer populations of **2** generated here were used to develop a novel feature extraction technique for fuzzy relational clustering of molecular conformations of flexible molecules [24, 25].

Methods

All calculations were carried out on Silicon Graphics Origin 2000 workstations at the New Jersey Institute of Technology using either version 6.9 or 7.1 of the SYBYL molecular modeling program.

Analogs **2** and **3**

Protonation of analogs

Studies of the pH dependence of dopamine binding to the DAT [26] indicate that dopamine most likely binds in the protonated state. In contrast, similar studies of WIN 35,428 [27], a cocaine analog, indicate that the protonated and neutral species have similar binding affinities. Our recent studies [28] on the conformational potential energy surface (PES) of the dopamine reuptake inhibitor methylphenidate (**4**, Fig. 1) indicate that the local minima on the PES of the protonated species are fewer in number but located in the same general region of conformational space as those of the neutral species. It was found that conformers which correspond to the neutral and protonated local energy minima could be grouped roughly into the same conformational families. Since it is not clear whether the GBR 12909 analogs bind to the DAT in the neutral or protonated state, and since protonation seems to lead to fewer conformational energy minima, in order to simplify the number of conformations that needed to be analyzed, calculations were carried out for only the protonated forms of analogs **2** and **3**.

Since **2** is a piperazine, it is possible that either nitrogen could be protonated. Molecular orbital theory was used to determine the preferred site of protonation. Given the large size of the GBR 12909 molecule, two somewhat smaller model compounds were used for initial calculations: compound A (GBR 12909 with hydrogens replacing the three aromatic rings) and compound B (GBR 12909 with a hydrogen replacing only the phenyl ring). The phenyl rings were held frozen in the geometry optimizations of compound B and GBR 12909 described below. Compound A was constructed in an extended conformation. Initial geometry optimization was carried out with the HF/6-31G (d) basis set, followed by final geometry optimization at the HF/6-31G++(d,p) level using the Gaussian 03 [29] program. The relative energies (in kcal mol^{-1}) of protonation at the N1, N4, and O atoms of compound A were calculated to be 0.00, 1.87, and 39.39, respectively, with the HF/6-31++G(d,p) basis set. Compound B was constructed from compound A and geometry optimization was carried out with both basis sets. The relative energies (in kcal mol^{-1}) of protonation at the N1, N4, and O atoms of compound B were calculated to be 0.00, 1.94, and 35.96, respectively, with the HF/6-31++G (d,p) basis set, and 0.00, 1.89, and 36.70 with the HF/6-31G

(d) basis set. These results indicate that the N1 is favored over N4 as the site of protonation by about 2 kcal mol^{-1}, and that protonation on the ether oxygen is disfavored. Since both basis sets gave almost the same results for the relative energy of protonation, only the less diffuse HF/6-31G(d) basis set was used for the calculations on GBR 12909. GBR 12909 was built from compound B and its geometry was optimized. The relative energies (in kcal mol^{-1}) of protonation at the N1 and N4 atoms of GBR 12909 were calculated to be 0.00 and 3.07, respectively, with the HF/6-31G(d) basis set. Oxygen protonation was not considered.

Geometry optimization of the HF/6-31G(d)-optimized GBR 12909 structure with the AM1 semiempirical molecular orbital method [30], followed by calculation of the solvation energy using the AM1/SM5.4 method [31] with the PC SPARTAN program (available from Wavefunction, Inc.), showed N1 protonation to be favored over N4 by 0.37 kcal mol^{-1} in water. This is the same nitrogen that was shown to be required for the DAT binding by Dutta et al. [6]. For these reasons, analog **2** was protonated at the nitrogen proximal to the naphthalene moiety, as was **3**.

Generation of conformer populations by random search conformational analysis

a. *Protocol*. Conformational analysis was carried out using the Random Search [32] (RS) option in SYBYL with the force fields, charge sets, and solvent models described below. The RS algorithm is designed to locate the local minima on the conformational PES. It randomly alters the values of the chosen torsional angles, and then optimizes the geometry by minimizing the energy of the molecule at each new conformation. The chosen torsional angles (A1, A2, B1–B6) are indicated in Fig. 1 for analogs **2** and **3**.

Before constructing the analogs, molecular orbital theory was used to evaluate the optimal placement of side chains on an individual piperazine or piperidine ring. Methyl groups were substituted at the N1 and N4 (piperazine) or C4 (piperidine) locations in the axial–axial (aa), equatorial–axial (ea), axial–equatorial (ae, piperidine), and equatorial–equatorial (ee) orientations to produce seven model compounds. The geometry of each model was optimized using the HF/6-31G* basis set. The relative energies (in kcal mol^{-1}) for the piperazines (ee: 0.00, ea: 3.86, aa: 8.30) and piperidines (ee: 0.00, ea: 2.37, ae: 3.56, aa: 6.09) indicate that the diequatorial conformations are the lowest energy structures. For this reason, in the construction of **2** and **3**, the side chains were attached to the central ring in the equatorial position.

For each search, the rings were held fixed as aggregates and the geometry of the starting conformer was optimized using the Powell [33] minimization method. One thousand search iterations were carried out. At each step in the iteration, the eight torsional angles were randomly altered and the resulting structure was optimized again using the Powell minimization method. A convergence threshold of 0.05 and a nonbonded distance cutoff of 8.0 Å were used for each random search. A conformer was accepted into the ensemble of conformers if it met the following energy and root mean square (RMS) criteria: (1) its RMS distance difference compared to all other conformers was at least 0.20 Å, and (2) its energy was within 20 kcal mol^{-1} of the energy of the conformer identified as having the lowest energy at that particular step in the random search. The random search procedure ended after 1,000 steps. The energy cutoff was purposely set high in order to thoroughly probe the PES of the molecule. The relative energy of each conformer was calculated by subtracting the absolute energy of the global energy minimum (GEM) conformer from that of each conformer. The parameters used for the various random search runs are summarized in Table 2.

b. *Force fields, charges, solvent models*. For both **2** and **3**, four different RS runs were made using the following combinations: the Tripos force field and Gasteiger–Hückel atomic charges (in vacuum and solvent) with the default distance-dependent dielectric function; the MMFF94 force field and associated MMFF94 atomic charges (in vacuum and solvent) with the default constant dielectric function. The dielectric constant value was set equal to 1 for the vacuum phase and 80 for the solvent calculations.

Analysis of conformer populations

a. *Molecular shape*. The distance of closest approach between rings on the A- and B- sides was used to give a gross indication of the extent to which the molecule assumes a "folded" shape. The SYBYL molecular modeling program was used to identify the centroid of each of the phenyl rings and ring 1 of the naphthalene ring (Fig. 2a). For each conformation, the distances between the centroid of each phenyl ring (rings 3 and 4) and that of ring 1 of naphthalene were calculated as D_{13} or D_{14}, respectively. The lesser of these two distances, defined as LD, was defined as the distance of closest approach of the napthalene and bisphenyl moieties.

Virtual torsional (VT) angles were defined in order to give an estimate of the degree to which the naphthalene and phenyl rings are offset (or "swung away") from each other. The VT angle was defined by the following four points: (1) the centroid of ring 1 of the naphthalene ring, (2) the nitrogen of the piperazine (or piperidine) ring proximal to

Table 2 Random search parameters

Maximum cycles	1000
Energy cutoff	20 kcal/mol
Convergence threshold	0.05
Maximum iterations	1000
Minimum hits	6
Check chirality	Yes
Check symmetry	Yes
Force field	Tripos or MMFF94
Charges	Gasteiger–Hückel or MMFF94
Dielectric function	Distance dependent—Tripos default
	Constant—MMFF94 default
Dielectric constant	1.0 (vacuum) or 80 (water)
NB cutoff	8.0 Å
Aggregates	On (phenyl rings, naphthalene ring, piperazine/piperidine ring)

the naphthalene ring, (3) the nitrogen (for **2**) or carbon (for **3**) to which the bisphenyl side chain is attached, and (4) the centroid of either phenyl ring. These points are connected by the dotted lines on analog **2** in Fig. 2b, and indicate the virtual torsional angles (VT_{13} and VT_{14}) that define the relative orientation of the napthalene and bisphenyl rings. Conformers were classified into shapes based on the following LD/VT combinations, with LD given in angstroms and VT_{13} or VT_{14} given in degrees. Examples of typical shapes are given in Fig. 3.

$$C : LD \leq 5, \ and \ VT_{13} \ or \ VT_{14} \leq \pm 45$$
$$V : 5 < LD \leq 7 \ and \pm 45 < VT_{13} \ or \ VT_{14} \leq \pm 75$$
$$U : 7 < LD \leq 12 \ and \pm 75 < VT_{13} \ or \ VT_{14} \leq \pm 100$$
$$S : 7 < LD \leq 12 \ and \pm 100 < VT_{13} \ or \ VT_{14} \leq \pm 180$$
$$I : D_{13} \ or \ D_{14} > 12.$$

b. *Energy profiles*. The local energy minimum conformations identified by each RS run were assigned to energy "bins" (in units of kcal mol^{-1}) on a histogram as follows: 0–4 bin: 0≤ relative energy <4, 4–8 bin: 4≤ relative energy <8, and so on. Histogram energy profiles were compared for the different RS runs.

c. *Conformer populations in torsional angle space*. Due to the impossibility of viewing the results in eight-dimensional torsional angle space, the local energy minima from each RS run were plotted in two-dimensional torsional angle space for all pairs of consecutive torsional angles: (A1, A2), (B1, B2), ..., (B4, B5), (B4, B6), and (B5, B6). As will be seen below, the two force fields resulted in a significant difference in the range of B4 values taken on by the conformer populations of **2** and **3**. Note that the torsional angle B4 involves rotation around a C(sp^3)–O(sp^3) bond. To examine this difference in detail, models of the B-side of the analogs were constructed, and relevant regions of their PES were studied with both molecular mechanics and molecular orbital techniques.

Model compounds

Two model compounds (**5** and **6**; Fig. 1) were constructed to study the influence of the bisphenyl moiety on C(sp^3)–O(sp^3) internal rotation. Note that **5** has the C(sp^3)–O(sp^3)

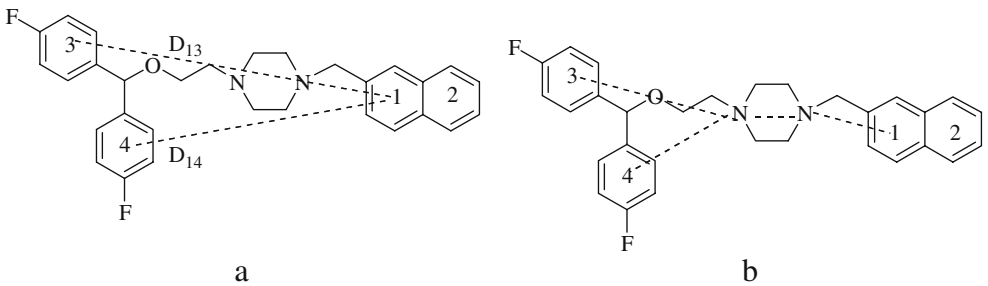

Fig. 2 Definitions of the closest distance and virtual angles. **a** Distance of closest approach (LD) between the A- and B- sides is the lesser of the two distances D_{13} and D_{14}. D_{13} is the distance between the centroids of rings 1 and 3; D_{14} is the distance between the centroids of rings 1 and 4. **b** Points used to define virtual torsion angles: VT_{13}=1–N–N–ring 3 centroid and VT_{14}=1–N–N–ring 4 centroid

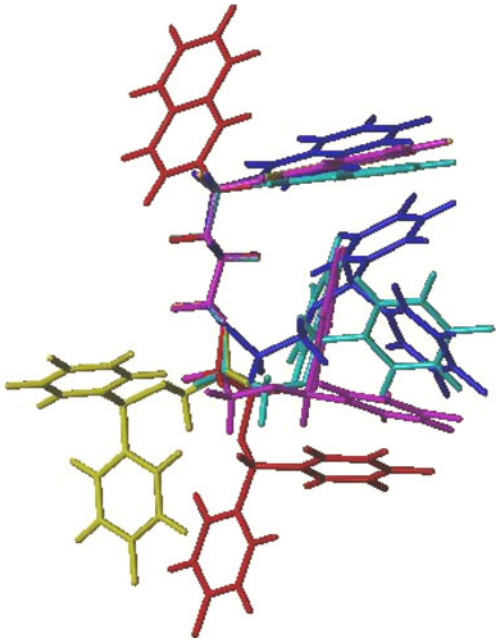

Fig. 3 Typical conformers representative of each shape: *blue*, C; *cyan*, V; *magenta*, U; *yellow*, S; *red*, I. The *yellow S shape* overlaps the *magenta U shape* in the upper right-hand portion of the figure

bond proximal to the bisphenyl group, as in **2** and **3**, so that torsional angle 2 is a model for B4; **6** has one less phenyl ring than **5**.

Generation of conformer populations by random search conformational analysis

Vacuum-phase RS conformational analysis was carried out for **5** and **6** using the protocol described above and the search parameters in Table 2. All four torsional angles were allowed to vary for **5** and **6**. The conformer populations were plotted in (torsional angle 2, torsional angle 3) space.

Calculation of the potential energy surface by grid search conformational analysis

Since RS only locates the minima on the conformational PES, a vacuum-phase grid search was also carried out on both **5** and **6** in order to obtain additional details about the PES landscape. For each model compound, torsional angles 2 and 3 were altered in 10° increments, forming a grid of torsional angle points. At each grid point, the energy of the molecule was minimized using the chosen force field, holding torsional angles 2 and 3 constant. Each PES grid was plotted using the Origin Pro 7 SR4, Version 7.0552 (B552) package (available from the OriginLab Corporation, Northampton, MA, USA).

Molecular orbital calculations

As will be seen in the "Results" section, for **5**, the largest difference between the conformational energies calculated by the two force fields was found in the region where torsional angle 2 was between −60° and 60°. Not only were the barriers to internal rotation significantly different, but also the conformational energy minima calculated by the two force fields were found at very different values of torsional angle 2 in this range. The same result was noted in the RS output for **2** and **3** for B4: conformational energy minima calculated by the two force fields were found at very different values of B4 for B4 between −60° and 60˚.

To probe these differences, molecular orbital calculations were carried out on **5** using the Gaussian 03 program. A "slice" was taken through the potential energy surface of **5** by freezing torsional angle 3 at −30°. Then torsional angle 2 was incremented in 30° steps and the energy was minimized at each point using the HF/6–31G(d) and B3LYP/6–31G(d) basis sets in the vacuum phase. The C–O rotational barrier and the location of the minima with respect to torsional angle 2 in the molecular orbital results were compared to the molecular mechanics grid search results for the rotation of torsional angle 2 with torsional angle 3 frozen at −30°. It should be noted that these molecular orbital calculations are not meant to provide a definitive calculation of C–O internal rotation, since MMFF94 was parameterized to a much higher level of theory [15].

Results

Analogs **2** and **3**

Conformer populations from random search conformational analysis

The RS algorithm identified more than 700 distinct local energy minimum conformations for the piperazine, **2**, and the piperidine, **3**, with the Tripos force field in both vacuum and solvent (vacuum: 728 for **2** and 718 for **3**, solvent: 735 for **2** and 733 for **3**). With MMFF94, the RS algorithm found more than 600 distinct local energy minimum conformations in vacuum (643 for **2** and 632 for **3**) and more than 750 in solvent (791 for **2** and 780 for **3**).

a. *Energy profiles*. Figure 4 shows the number of conformers in each energy bin for **2** and **3** for the Tripos and MMFF94 random search results. The percent distributions of conformers among energy bins (i.e., the conformer energy profile) are very similar for **2** and **3** in the MMFF94 force field, but somewhat different in

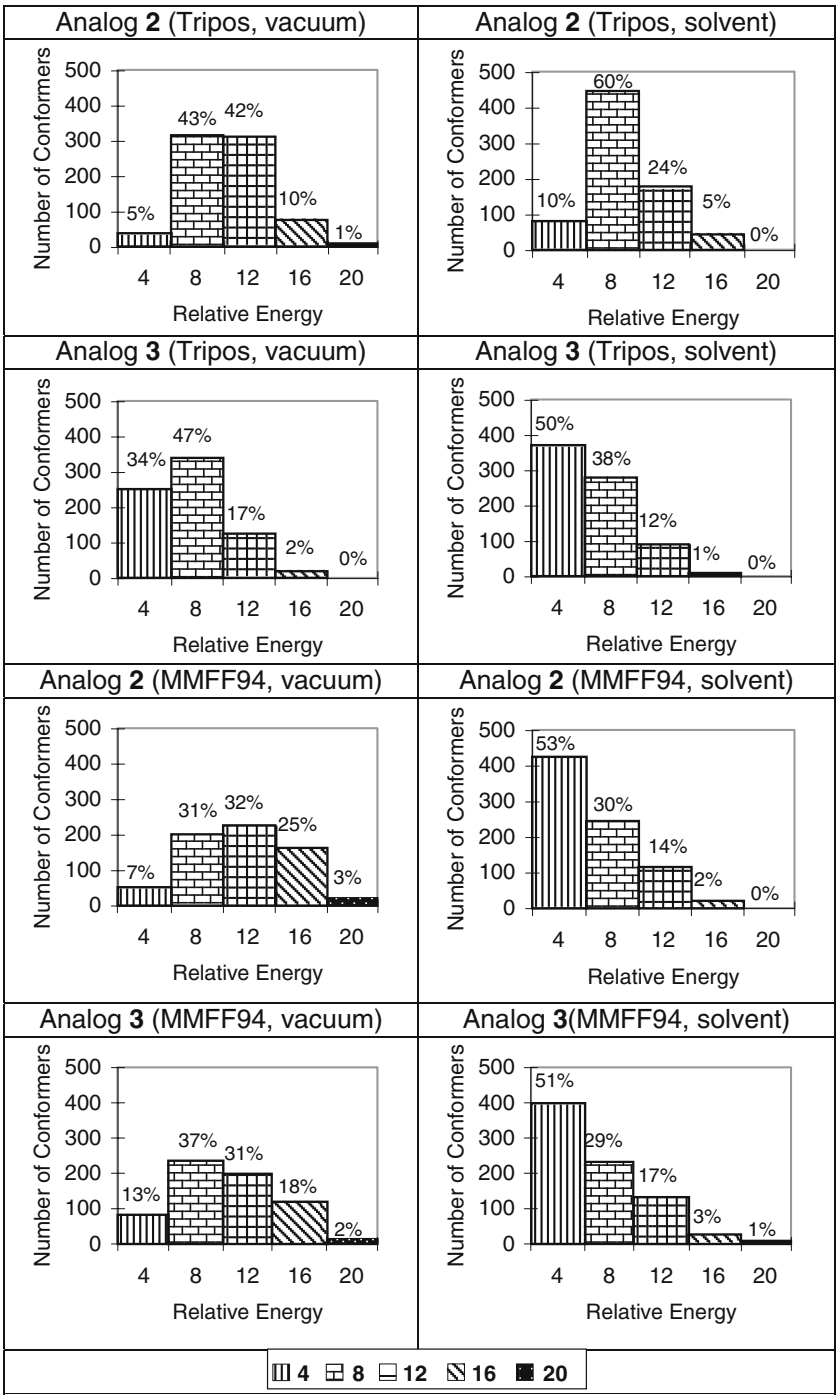

Fig. 4 Energy distributions of conformers with the Tripos and MMFF94 force fields in vacuum and solvent. Relative energies in kcal mol^{-1}

the Tripos force field. The MMFF94 vacuum phase conformer profile of **2** is similar to that of **3**, as is the MMFF94 solvent phase profile. However in the Tripos force field, **3** has a significantly larger percentage of conformers in the 0–4 kcal mol^{-1} energy bin than **2** in both vacuum and solvent phases. In all cases, solvent significantly increases the percentage of conformers in the 0–4 kcal mol^{-1} energy bin compared to the vacuum phase results.

b. *Molecular shape*. Tables 3, 4, 5 and 6 give the numbers of C, V, U, S and I shapes of **2** and **3** in each of the energy bins, as well as the total number of conformers of each shape and the total number in each energy bin. For the Tripos force field in vacuum and solvent (Tables 3 and 4), **2** has more C shapes than **3** by an order of magnitude. The number of C shapes in vacuum and solvent for the MMFF94 force field (Tables 5 and 6) is negligible for both analogs. The I shape predom-

Table 3 Energy distributions of molecular shapes; Tripos force field, vacuum phase

Analog **2**	0–4[a]	4–8[a]	8–12[a]	12–16[a]	16–20[a]	Total/shape[b]
C	17	12	1	0	0	30
V	7	40	9	4	0	60
U	10	111	108	16	3	248
S	0	49	22	3	0	74
I	0	99	167	48	2	316
Total/bin	34	311	307	71	5	728
Analog **3**	0–4[a]	4–8[a]	8–12[a]	12–16[a]	16–20[a]	Total/shape[b]
C	1	0	0	0	0	1
V	27	4	3	1	0	35
U	103	71	20	2	0	196
S	68	53	13	2	0	136
I	48	207	85	10	0	350
Total/bin	247	355	121	15	0	718

[a] kcal mol^{-1}. Columns contain number of conformers in each energy bin

[b] Total number of conformers of each shape. See text for definitions

inates in all cases. Its percentage varies from about 40–50% (Tripos) to 60% (MMFF94) of the total number of conformers for both **2** and **3**. The U shape is the second most favored shape, with about 25–35% of the total number of conformers for both force fields for both **2** and **3**. Comparisons of Table 3 with Table 4 and Table 5 with Table 6 show that the inclusion of implicit solvent has no effect on the molecular shape profile (i.e., the distribution of conformers among molecular shapes).

c. *Conformer populations in torsional angle space*. Plots of the conformational energy minima in torsional angle space that show no significant differences between the force fields (i.e., (B2, B3) and (B3, B4)) are given in the "Electronic supplementary information." The (A1, A2) plot is discussed below as an example of this case. Since B5 and B6 are correlated due to the constraints of the structure of the bisphenyl group, a plot in (B4, B6) or (B5, B6) space gives no new information compared to that in (B4, B5) space, so the former are given in the "Electronic supplementary information" and the latter is discussed below. Large differences between the force fields were noted for the (B1, B2) plot, and these are detailed below.

(1) *(A1, A2) torsional angle space*. Figure 5 plots the conformational energy minima from the random search runs in (A1, A2) torsional angle space. The minima are color-coded by relative energy as described in the figure legend. The figure shows that all the patterns are very similar, indicating that the local minima on the A-sides of **2** and **3** are located in very similar regions of (A1, A2) space for the Tripos and MMFF94 results in vacuum and solvent. In all cases, the conformational energy minima cluster into groups (i.e., at A1 = ±60°, ±180°) that have values of A1 that differ by approximately 120°. From the structure of **2** (Fig. 1), it can be seen that the three clusters correspond to the staggered conformations that are the conformational energy minima for rotation around the N(sp^3)–C(sp^3) bond

Table 4 Energy distributions of molecular shapes; Tripos force field, solvent phase

Analog **2**	0–4[a]	4–8[a]	8–12[a]	12–16[a]	16–20[a]	Total/shape[b]
C	24	6	0	0	0	30
V	24	29	7	1	0	61
U	23	172	68	14	0	277
S	6	52	19	1	2	80
I	0	183	80	24	0	287
Total/bin	77	442	174	40	2	735
Analog **3**	0–4[a]	4–8[a]	8–12[a]	12–16[a]	16–20[a]	Total/shape[b]
C	1	2	0	0	0	3
V	30	9	3	0	0	42
U	135	62	17	4	0	218
S	47	23	2	0	0	72
I	154	179	64	1	0	398
Total/bin	367	275	86	5	0	733

[a] kcal mol^{-1}. Columns contain number of conformers in each energy bin

[b] Total number of conformers of each shape. See text for definitions

Table 5 Energy distributions of molecular shapes; MMFF94 force field, vacuum phase

Analog **2**	0–4[a]	4–8[a]	8–12[a]	12–16[a]	16–20[a]	Total/shape[b]
C	0	3	0	0	0	3
V	17	31	10	8	0	66
U	16	59	38	49	8	170
S	1	24	6	5	0	36
I	14	80	168	96	10	368
Total/bin	48	197	222	158	18	643
Analog **3**	0–4[a]	4–8[a]	8–12[a]	12–16[a]	16–20[a]	Total/shape[b]
C	0	0	0	0	0	0
V	18	15	4	2	0	39
U	37	89	42	28	3	199
S	3	16	1	2	0	22
I	21	111	149	84	7	372
Total/bin	79	231	196	116	10	632

[a] kcal mol^{-1}. Columns contain number of conformers in each energy bin

[b] Total number of conformers of each shape. See text for definitions

of the A1 torsional angle. The pattern of minima along the A2 axis is more complex and corresponds to staggered conformations which are the conformational energy minima for rotation around the C(sp^3)–C(sp^2) bond of the A2 torsional angle. Similar behavior was seen in the conformational PES of methylphenidate, which also has a piperazine ring separated from an aromatic ring by a methylene group [28].

Figure 5 also shows that the location of the GEM conformer (indicated by a large circle) is influenced by both solvent and force field. Except for the MMFF94 results for **3**, for each analog in each force field, the GEM conformer from the solvent study is located in a different region of (A1, A2) space than that from the vacuum phase study. Also, except for the Tripos and MMFF94 vacuum phase results for **3**, the GEM conformer from the Tripos results is located in a different region of torsional angle space than that for the MMFF94 results.

(2) *(B1, B2) torsional angle space*. Figure 6 shows the local minima of **2** and **3** in (B1, B2) torsional angle space. All cases, except the Tripos vacuum and solvent phase results for **2**, show nine well-defined minima which result from combination of the staggered conformations, which are the minima for rotation around the N(sp^3)–C(sp^3) bond (in **2**) or C(sp^3)–C(sp^3) bond (in **3**) in the B1 torsional angle (at B1=±60°, ±180°), with those that are the minima for rotation around the C(sp^3)–C(sp^3) bond in B2 (at B2=±60°, ±180°). In contrast, the Tripos results for **2** give minima that take on a range of B1 values not seen in the Tripos results for **3** nor in the MMFF94 results for **2** and **3**. Since **2** and **3** differ only by a tertiary amine nitrogen versus a tetrahedral carbon in the B1 torsional angle, the difference in the conformer populations of **2** and **3** may be due to differences in how the force fields treat a tertiary amine nitrogen atom type and, ultimately, in the effect of that nitrogen

Table 6 Energy distributions of molecular shapes; MMFF94 force field, solvent phase

Analog **2**	0–4[a]	4–8[a]	8–12[a]	12–16[a]	16–20[a]	Total/shape[b]
C	0	0	0	0	0	0
V	29	14	4	0	0	47
U	96	50	40	6	0	192
S	20	12	8	1	0	41
I	274	165	62	10	0	511
Total/bin	419	241	114	17	0	791
Analog **3**	0–4[a]	4–8[a]	8–12[a]	12–16[a]	16–20[a]	Total/shape[b]
C	0	0	0	0	0	0
V	42	7	3	0	0	52
U	111	46	45	8	2	212
S	19	8	5	0	2	34
I	222	168	75	16	1	482
Total/bin	394	229	128	24	5	780

[a] kcal mol^{-1}. Columns contain number of conformers in each energy bin

[b] Total number of conformers of each shape. See text for definitions

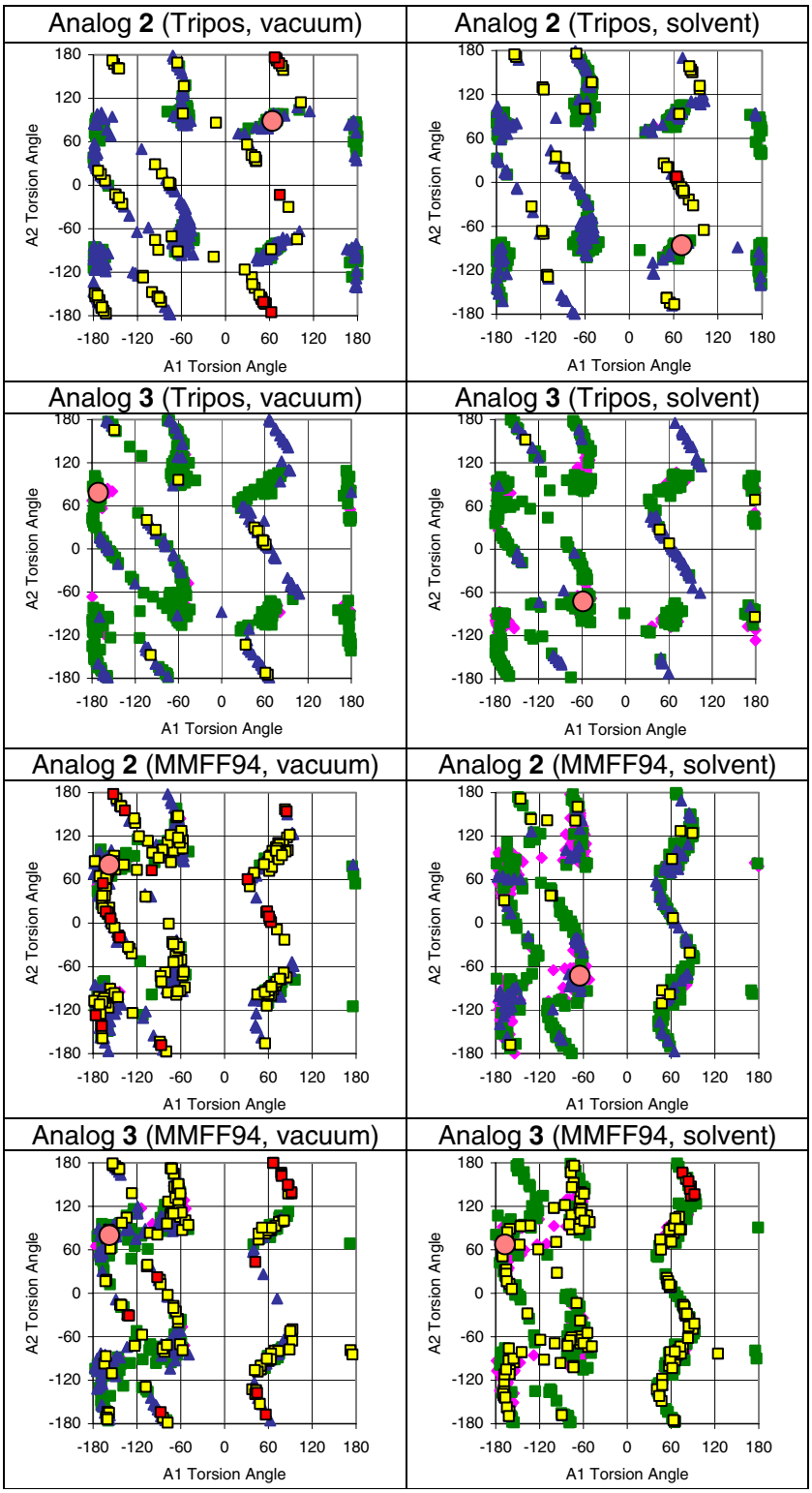

Fig. 5 Local minima of **2** and **3** in (A1, A2) space. Torsion angles are given in degrees. Minima are color-coded by energy in units of kcal mol^{-1}. GEM marked by a *circle*. Plot symbols: *pink diamond*, 0–4; *green box*, 4–8; *blue triangle*, 8–12; *yellow box*, 12–16; *red box*, 16–20

on N(sp^3)–C(sp^3) internal rotation. This is illustrated in Fig. 7. Using the conformer populations from the vacuum-phase results for both force fields, for each conformer Fig. 7 plots the distance of the nitrogen atom in B1 of **2** with respect to a plane formed by three neighboring carbon atoms, and compares it to a similar plot for the related carbon atom in **3**. The figure shows a distinctive difference in the pattern for the nitrogen of **2** in the Tripos versus MMFF94 force fields. In the Tripos

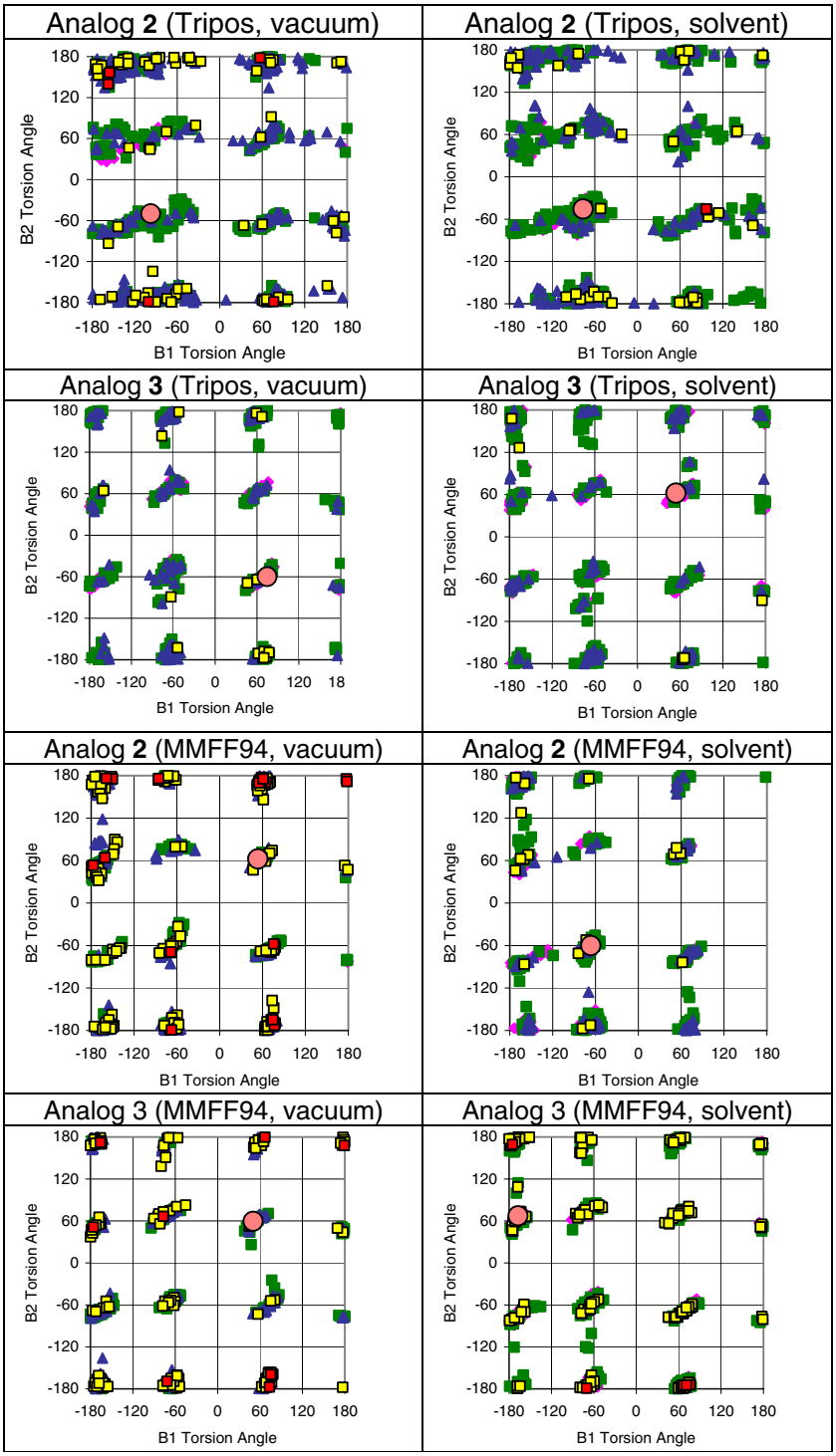

Fig. 6 Local minima of **2** and **3** in (B1, B2) space. Torsion angles are given in degrees. Minima are color-coded by energy in units of kcal mol^{-1}. GEM marked by a *circle*. Plot symbols: *pink diamond*, 0–4; *green box*, 4–8; *blue triangle*, 8–12; *yellow box*, 12–16; *red box*, 16–20

case (Fig. 7a), about 15% of the conformers have a somewhat planar nitrogen (arbitrarily defined as a nitrogen with a distance with respect to the plane of between −0.30 and 0.30 Å). For the MMFF94 results for **2** (Fig. 7c), essentially 100% of the conformers have a tetrahedral nitrogen. This seems to indicate that, during the RS procedure, the Tripos force field allows the nitrogen to attempt to "flatten out," even though the B-side side chain was held fixed in the equatorial position. In contrast, the MMFF94 force field keeps the nitrogen tetrahedral. Figure 7b and d show that the related carbon atom in **3** remains tetrahedral during the RS with both force fields. Similar trends are seen in the solvent-phase results (not shown).

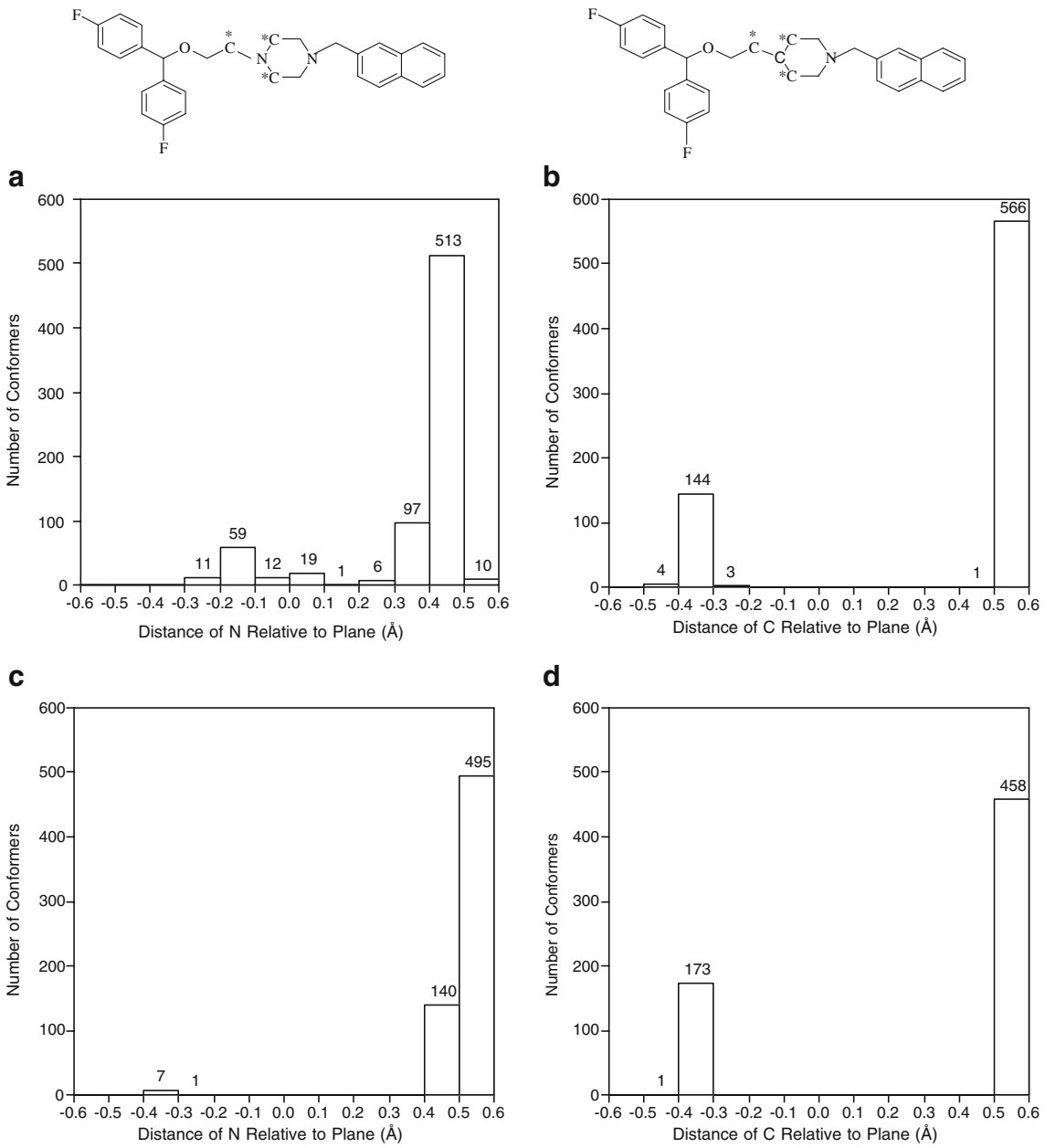

Fig. 7 Number of conformers with distance of N or C relative to the plane of three carbons identified on the molecular structure. **a 2**, Tripos in vacuum phase; **b 3**, Tripos in vacuum phase; **c 2**, MMFF94 in vacuum phase; **d 3**, MMFF94 in vacuum phase. Conformers that have a distance greater than 0 and less than or equal to 0.1 are assigned to the bin labeled 0.1, and so on

(3) *(B4, B5) torsional angle space*. Figure 8 shows the local minima of **2** and **3** in (B4, B5) torsional angle space. There are striking differences between the Tripos and MMFF94 results. In the Tripos case, conformers cluster along the B4 values of −60° and 60°, with few conformers in the B4 range between −60° to 60°. The MMFF94 results present the opposite picture, with most conformers found for values of B4 between −60° and 60°. This difference between the two force fields with respect to B4 is also demonstrated in the plots of the local minima of **2** and **3** in (B3, B4) and (B4, B6) space (see "Electronic supplementary information"). Note that the B4 torsional angle involves rotation around the $C(sp^3)$-$O(sp^3)$ bond. Although the B3 torsional angle also involves rotation around the $C(sp^3)$-$O(sp^3)$ bond, in this case the two force fields agree that the minima for **2** and **3** are found for values of B3 close to −60° and 60°, rather than between −60° and 60° (see plots of minima in (B2, B3) and (B3, B4) space in the "Electronic supplementary information"). Since B4 is proximal to the bisphenyl

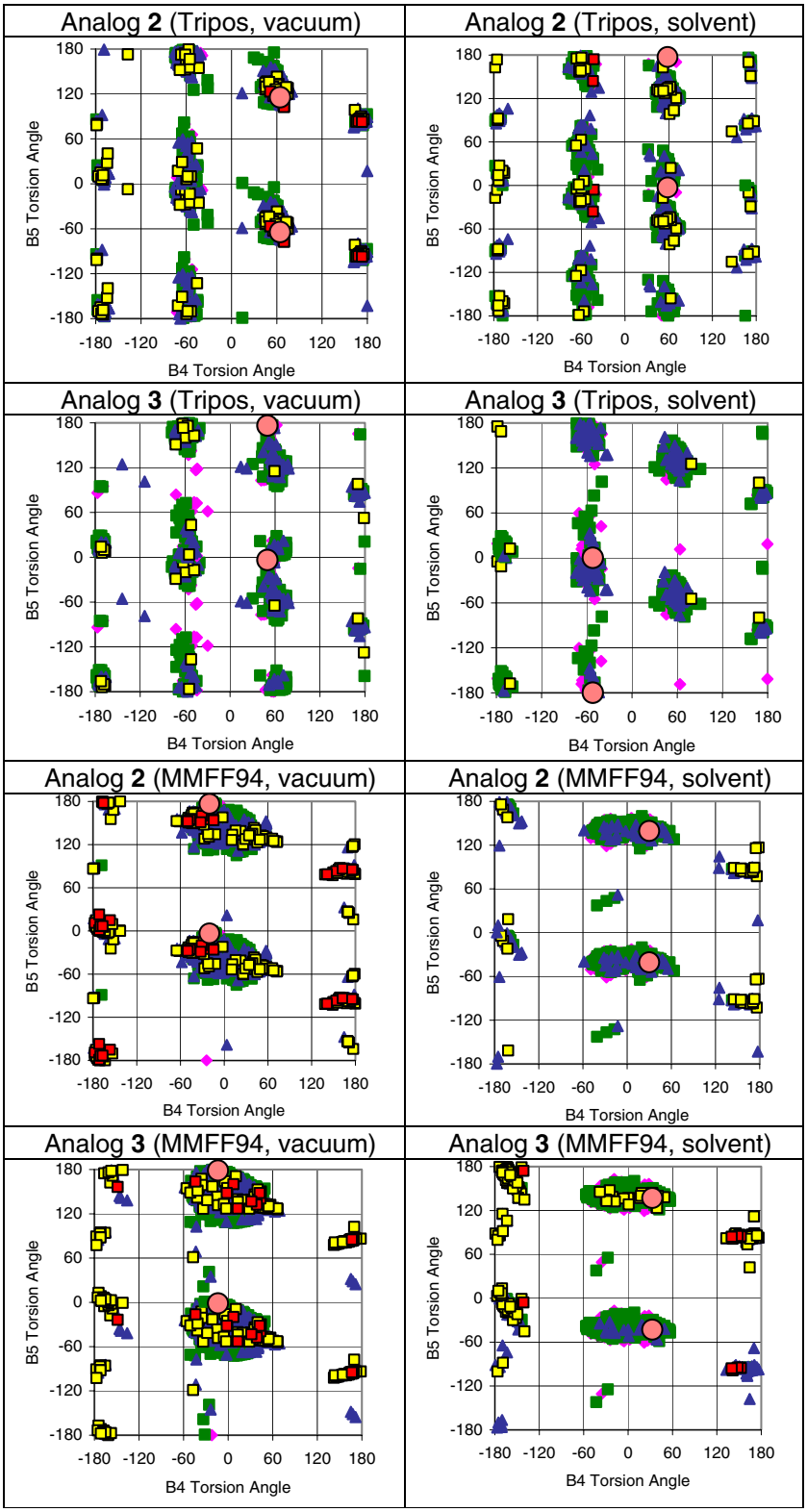

Fig. 8 Local minima of **2** and **3** in (B4, B5) space. Torsion angles are given in degrees. Minima are color-coded by energy in units of kcal mol^{-1}. GEM marked by a *circle*. Plot symbols: *pink diamond*, 0–4; *green box*, 4–8; *blue triangle*, 8–12; *yellow box*, 12–16; *red box*, 16–20. The GEM structure appears twice due to the symmetry of the molecule to rotation of the phenyl ring around the B5 torsional angle

moiety, whereas B3 is an additional bond length away, it is possible that the presence of the two phenyl rings affects the minima for C(sp^3)–O(sp^3) rotation differently in the Tripos and MMFF94 force fields. In order to investigate these issues in more detail, molecular mechanics and molecular orbital calculations were carried out on model compounds. The results are described below.

Model compounds

The model compound studies were designed to investigate the effect of the bisphenyl moiety on internal rotation by comparing rotation around the C–O bond in **5** to that in **6**. Torsional angle 2 in **5** is the equivalent of B4 in **2** and **3**. Figure 9 displays the results of the molecular mechanics grid search calculations of the PESs of **5** and **6**. The low-energy conformers identified by the RS calculation are shown as white squares on the grid. Comparison of Fig. 9a and b shows a general similarity in the location of regions of high and low energies for **5** in the two force fields. Both force fields find high-energy regions for torsional angle 2 between −180° and −120°, as well as between 90° and 180°. Both force fields show regions of low energy for torsional angle 2 equal to ±60°. However, the MMFF94 force field displays a broad region of low energy for **5** for torsional angle 2 between −60° and +60°, while the Tripos force field shows a much higher energy range in this region. Comparison of Fig. 9a and c shows that removing one phenyl ring from **5** to give **6** has little effect on the characteristics of the Tripos PES. In contrast, comparison of Fig. 9b and d shows that removal of one phenyl ring leads to significant broadening of the low-energy region on the MMFF94 PES. Therefore, it seems that the bisphenyl moiety has a larger effect on the internal rotation of a proximal C–O bond in the MMFF94 force field than the Tripos force field.

Molecular orbital calculations

Figure 10 plots the results for C–O internal rotation for **5** at the HF/6-31G(d) and B3LYP/6-31G(d) levels with torsional angle 3 set equal to −30°. For comparison purposes, the "slice" through the PES of **5** for torsional angle 3 equal to −30° from Fig. 9a and b is also shown on the graph. Figure 10 shows that both the Hartree Fock (HF) HF/6-31G (d) and density functional theory (DFT) B3LYP/6-31G(d) techniques give very similar results, with the global energy minimum falling at −60°, local minima at −150° and 30°, a low rotational barrier (1.52 kcal mol^{-1} for HF, 1.89 kcal mol^{-1} for DFT) at 0°, and a very high barrier at

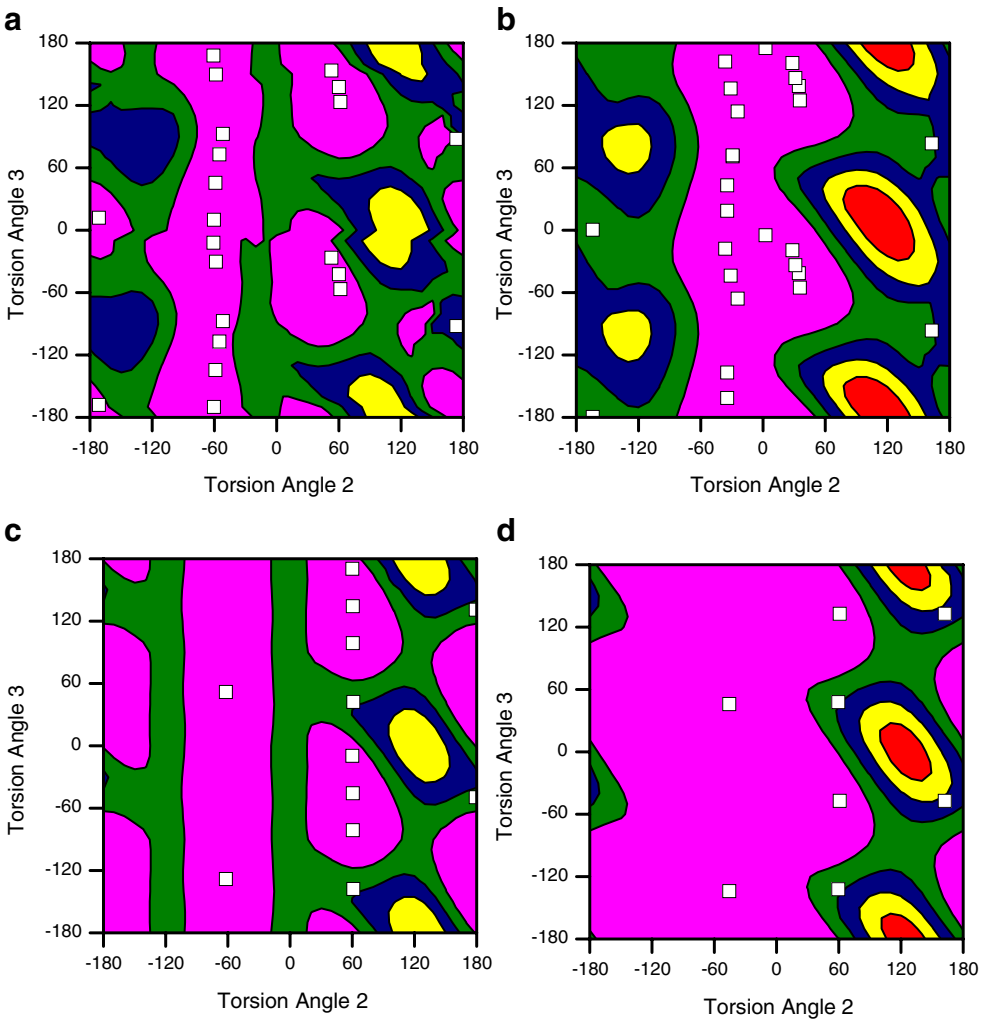

Fig. 9 Vacuum-phase potential energy surfaces of model compounds. Contours are color-coded by relative energy (kcal mol^{-1}) as follows: *magenta*, 0–4; *green*, 4–8; *blue*, 8–12; *yellow*, 12–16; *red*, 16–20. **a 5**, Tripos; **b 5**, MMFF94; **c 6**, Tripos; **d 6**, MMFF94. Minima obtained from random searches for corresponding model compounds are shown as white squares

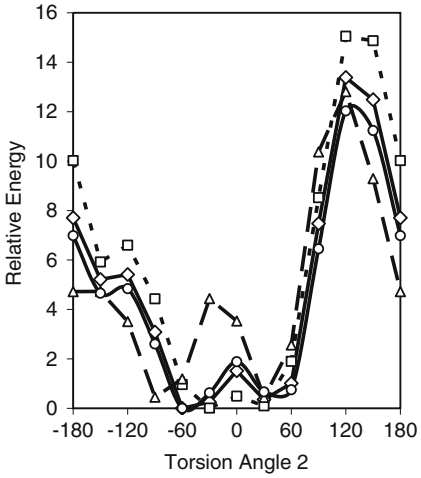

Fig. 10 Rotational barrier of torsional angle 2 of **5** (vacuum phase), with torsional angle 3 fixed at −30°. *Solid line with diamonds*, HF/6-31G(d); *solid line with circles*, B3LYP/6-31G(d); *dashed line with squares*, MMFF94 force field; *broken line with triangles*, Tripos force field. Relative energies in kcal mol^{-1}

120°. Overall, the molecular mechanics results are qualitatively similar to the molecular orbital results. However, there are some significant differences in the PES for torsional angle 2 between −60° and 60°. In contrast to the molecular orbital results, the MMFF94 force field locates the minima at −30° and 30°, with a much smaller barrier (only 0.49 kcal mol^{-1}) at 0°. The Tripos force field, however, gives a value at 0° (3.53 kcal mol^{-1}) which is significantly higher than the molecular orbital and MMFF94 results, and locates the minima at −90° and 30°, with a barrier at −30° of 4.44 kcal mol^{-1}. This explains why so many of the MMFF94 RS conformers of **2** and **3** are found in the region with B4 between −60° and 60° in Fig. 8, whereas the Tripos results tend to cluster around B4=±60° with no conformers found at B4=0°.

Discussion

Effect of implicit solvent on conformer populations

In all cases, the inclusion of an implicit solvent model significantly increased the percentage of conformers in the 0–4 kcal mol^{-1} energy bin compared to the vacuum phase results and affected the location of the GEM conformer in torsional angle space, without changing the molecular shape profile of the conformer populations. It should be noted that MMFF94 was parameterized for use in molecular dynamics simulations with discrete water molecules [15], whereas MMFF94s was developed for use in energy minimization studies [20]. The two force fields give identical results for most systems and differ only in their treatment of resonance-delocalized trigonal nitrogen atoms [20]. This atom type is not found in the GBR 12909 analogs, making either force field a suitable choice for the present study. Although the MMFF94 force field was not validated for use with the implicit solvent model employed here, since this option is available in the popular molecular modeling program SYBYL, it is of some interest to note its effect on the conformer populations.

Effect of force field on conformer populations

To the best of our knowledge, the results of calculations with the Tripos force field and Gasteiger–Hückel charge set have never before been directly compared to those obtained with the MMFF94 force field for large, flexible molecules containing carbon, hydrogen, nitrogen and oxygen atoms, such as the GBR 12909 analogs considered here. Since the Tripos force field was constructed and validated without atomic charges [14], it is useful to compare its behavior with the Gasteiger–Hückel charge set, a frequent choice among SYBYL users, to that of the more recent and more extensively-validated MMFF94 force field [15–21].

MMFF94 was parameterized for a wide variety of pharmaceutically relevant chemical systems using both high-level ab initio molecular orbital theory [15–18] and experimental data [19]. The "core" parameterization involved, among other calculations, geometry optimization of 500 molecular structures at the HF/6-31G* level, 475 structures at the MP2/6-31G* level, and 380 structures at a higher level including electron correlation and triple zeta plus polarization basis sets. Conformational energies were calculated in 250 cases at the "MP4SDQ/TZP" level, i.e., triple zeta plus polarization calculations at a defined approximation to the MP4SDQ level of theory. Approximately 1200 torsional profile structures, obtained by rotating a given torsional angle by a specified increment, were calculated at the MP2/TZP level derived from MP2/6-31G*-optimized geometries. The MMFF94 parameters were determined in a "mutually consistent" fashion from all of the available data using an iterative procedure in which each type of parameter was optimized while using increasingly well-refined parameters for the other parameter types [15]. This is different from the "functional group" approach employed by most force fields, including Tripos, in which certain parameters are fit to a portion of the data and then frozen. MMFF94 also employs a unique functional form for describing the van der Waals interactions [15].

In contrast, the Tripos force field (without charges) was validated against X-ray structures by minimizing three cyclic hexapeptides, crambin, and 76 small organic molecules. Thermodynamic barriers were calculated for 17 different conformational energies, 12 stereoisomers, and 15 rotational barriers [14].

Parameterization of tertiary amine nitrogen

Several differences were noticed in the conformer populations generated by the two force fields. For example, MMFF94 gave very similar conformer energy profiles for **2** and **3**, in contrast to the results with the Tripos force field, for which **3** had a significantly larger proportion of conformers in the 0–4 kcal mol^{-1} energy bin than **2** (Fig. 4). Although for both force fields most conformers of **2** and **3** were found in the I shape, with the U shape being the second most favored, only the Tripos force field allowed some conformers of **2** to take on the C shape (Tables 3, 4, 5 and 6). Comparison of the plots of the conformer populations in torsional angle space shows that both force fields yielded similar plots for **2** and **3** in (A1, A2) space (Fig. 5), and similar plots for **3** in (B1, B2) space (Fig. 6). However, for **2**, the (B1, B2) plots in Fig. 6 show that the conformers took on a different range of values for B1 in the Tripos versus the MMFF94 force fields. It should be noted that for **2**, although A1 and B1 both involve internal rotation around an N(sp^3)–C(sp^3) bond, the nitrogen in A1 is protonated whereas the nitrogen in B1 is not. For **3**, B1 involves internal rotation around the C(sp^3)–C(sp^3) bond.

In our previous work, singular value decomposition applied to all eight torsional angles (A1, ..., B6) in the Tripos vacuum-phase conformer populations of **2** and **3** uncovered differences in how the data separated along certain principal components, and in which torsional angles were the chief contributors to those principal components [34]. This indicated an underlying difference in the conformer populations of **2** and **3** generated by the Tripos force field. Since **2** and **3** only differ by an unprotonated tertiary amine nitrogen versus a tetrahedral carbon at the same location in the B1 torsional angle, the difference in their conformer populations was attributed to the treatment of the tertiary amine nitrogen by the Tripos force field.

In the present work, plots of the distance of the B1 nitrogen of **2** and the corresponding B1 carbon of **3** with respect to the plane of their neighboring carbons (Fig. 7) show that the Tripos force field allowed a significant percentage (15%) of the conformers of **2** to have tertiary amine nitrogens that were somewhat planar, while both Tripos and MMFF94 kept the B1 carbon tetrahedral. It should be noted that various conformers of 23 different amines were used in the "core" parameterization of MMFF94, and that the root mean square deviation (in degrees) for 96 out-of-plane angles in the set of saturated amines was only 0.91 for MMFF94 compared to 57.5 for the MP2/6-31G* method [15]. Of the 76 small molecules tested with the Tripos force field, about half contained various types of amine nitrogens, but statistics were given only for the RMS errors in bond lengths, bond angles, and torsional angles for the dataset as a whole. It should be noted, however, that compared to MMFF94, the Tripos force field overestimates the N(sp^3)–C(sp^3) rotational barrier (following values in kcal mol^{-1}): methylamine (experiment, 1.98 [35]; Tripos, 2.8 [14]; MMFF94, 2.36 [18]), dimethylamine (experiment, 3.62 [35]; Tripos, 4.9 [14]; MMFF94, 3.52 [18]).

The difference in how the force fields treat a tertiary amine nitrogen atom type and, ultimately, the effect of that nitrogen on N(sp^3)–C(sp^3) internal rotation appears to be one source of difference in the conformer populations of **2** and **3**.

Proximity of bisphenyl moiety to C–O bond

The effect of the bisphenyl group on C(sp^3)–O(sp^3) internal rotation appears to be another source of difference between the force fields. The plot of the conformer populations of **2** and **3** in (B4, B5) space (Fig. 8) showed striking differences between the Tripos and MMFF94 force fields for behavior with respect to B4, whereas a similar plot in (B2, B3) space ("Electronic supplementary information") showed little difference between the force fields. Torsional angles B3 and B4 both contain a C(sp^3)–O(sp^3) bond, but B4 is proximal to the bisphenyl group, whereas B3 is one bond length further away (Fig. 1). Calculations on model compounds **5** and **6** showed that the MMFF94 force field is sensitive to the effect of the bisphenyl moiety on C–O internal rotation (Fig. 9). Although 25 types of aromatic and heteroaromatic molecules along with various conformers of 14 types of conjugated systems were used in the core parameterization of MMFF94, none contained the bisphenyl moiety. However, MMFF94 has been shown to reproduce the C(sp^3)–C(sp^2) rotational barrier (relevant to rotation around the B5 and B6 torsional angles in **2** and **3**) for ethylbenzene (experiment, 1.16 kcal mol^{-1}; MMFF94, 1.19 kcal mol^{-1}; "MP4SDQ/TZP," 1.10 kcal mol^{-1}) [18]. In the Tripos validation study, no bisphenyl group was contained in the 76 small molecules studied and no C(sp^3)–C(sp^2) rotational barrier was contained in the 15 torsional barriers studied. It should be noted that the two force fields use different torsional potential functions (Tripos, one term; MMFF94, three terms).

C–O internal rotation

Calculations of C(sp^3)–O(sp^3) internal rotation in the model compound **5** (Figs. 9 and 10) showed that the MMFF94 force field allows a broad region of low energy between −60° and 60°, with a very low barrier (0.49 kcal mol^{-1}) at 0°, in contrast to the high barrier (4.44 kcal mol^{-1}) at −30° noted with the Tripos force field. The HF/6-31G(d) and B3LYP/6-31G(d) calculations were in qualitative agreement

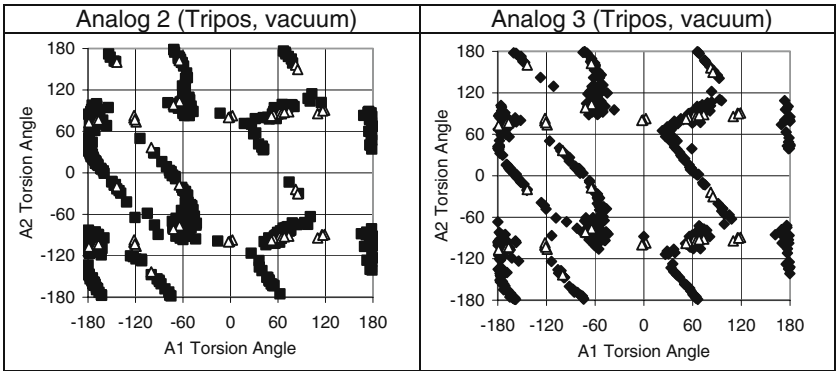

Fig. 11 Tripos force field vacuum-phase random search for local minima of **2** (*filled squares*) and **3** (*filled diamonds*) compared to local minima of **4** (*open triangles*) in (A1, A2) space. Torsional angles are given in degrees

with the MMFF94 results. It has been demonstrated that MMFF94, parameterized to the "MP4SDQ/TZP" level in conjunction with MP2/6-31G* optimized geometries, reproduces experimental conformational energies more accurately than the HF/6-31G* or MP2/6-31G* methods [18]. Of particular interest is the case of methylethyl ether, where the experimental value (in kcal mol^{-1}) for the *gauche-anti* energy difference is 1.5, the "MP4SDQ/TZP" result is 1.41, and the MMFF94 result is 1.5 [18]. MMFF94 also reproduces the experimental barrier for C–O rotation in dimethyl ether, whereas Tripos significantly overestimates it (following values in kcal mol^{-1}): experiment, 2.7 [35]; MMFF94, 2.43 [18]; Tripos, 4.2 [14]. Various conformations of 14 different ethers were used in the core parameterization of MMFF94 [15].

The difference in how the Tripos and MMFF94 force fields treat C(sp^3)–O(sp^3) internal rotation is responsible for the fact that, in the random search calculations, the local minima tend to collect at B4 values equal to ±60° for the Tripos force field, but at B4 values between −60° to 60° for the MMFF94 force field.

Comparison of conformer populations of **2** and **3** to methylphenidate

Figure 1 shows that methylphenidate, **4**, and the GBR 12909 analogs **2** and **3** share some pharmacophore features that are typical of most dopamine reuptake inhibitors: an aromatic group in close proximity to a basic nitrogen. Torsional angles A1 and A2 control the relative orientation of these important functional groups in **2**, **3**, and **4**. In order to compare the behavior of the A-sides of **2** and **3** to **4**, the conformer populations of all three (from random search calculations with the vacuum–phase Tripos force field, Gasteiger–Hückel charges, and distance-dependent dielectric function with dielectric constant set equal to 1) were plotted in (A1, A2) space. The conformer populations of **4** were taken from our previous work [28].

Figure 11 compares the locations of all the local minima of **2** and **3** to those of protonated **4** in (A1, A2) space. For simplicity of comparison to **4**, the minima of **2** and **3** are given the same symbol (filled squares), since Fig. 5 showed that the conformer populations of **2** and **3** have similar behavior in (A1, A2) space. Figure 11 shows that methylphenidate is far more conformationally restricted than **2** and **3** in (A1, A2) space. Although **4** has far fewer minima, they are located in roughly the same region of (A1, A2) space as those of **2** and **3**. This suggests that **2**, **3**, and **4** may share a common pharmacophore for DAT binding that involves the aromatic ring and nitrogen. However, the nitrogen in **4** is separated from the aromatic ring by three bonds, while the nitrogen in **2** and **3** is separated from the aromatic ring by only two bonds. For this reason, Fig. 12 compares the distance of the nitrogen from the centroid of the phenyl ring in **4** to the distance of the nitrogen in **2** and **3** from the centroid of ring 1 of naphthalene. A distance range of 3.75–4.35 Å is common to all three analogs. For **2** and **3**, all the conformers are in this range, while for **4**, 43% of the conformers are in this range. The fact that **2**, **3**, and **4** can orient their common pharmacophore elements in the same way suggests that the A-sides of the GBR 12909 analogs may attempt to bind to the DAT in a similar way to that of methylphenidate. However, the long B-sides of the GBR 129009 analogs may influence this interaction through a range of additional interactions with the DAT protein. A more definitive understanding of the DAT pharmacophore awaits the study of more rigid dopamine reuptake inhibitors, such as the recent study of rigid analogs of methylphenidate [36].

Summary

In summary, based on a comparison of the conformer populations of **2** and **3** generated by the Tripos and MMFF94 force fields, it seems that there are subtle differences in how a tertiary amine-type nitrogen is handled by the force fields. The force fields also differ significantly in their description of C–O internal rotation and the effect of the bisphenyl moiety on C–O internal rotation. These

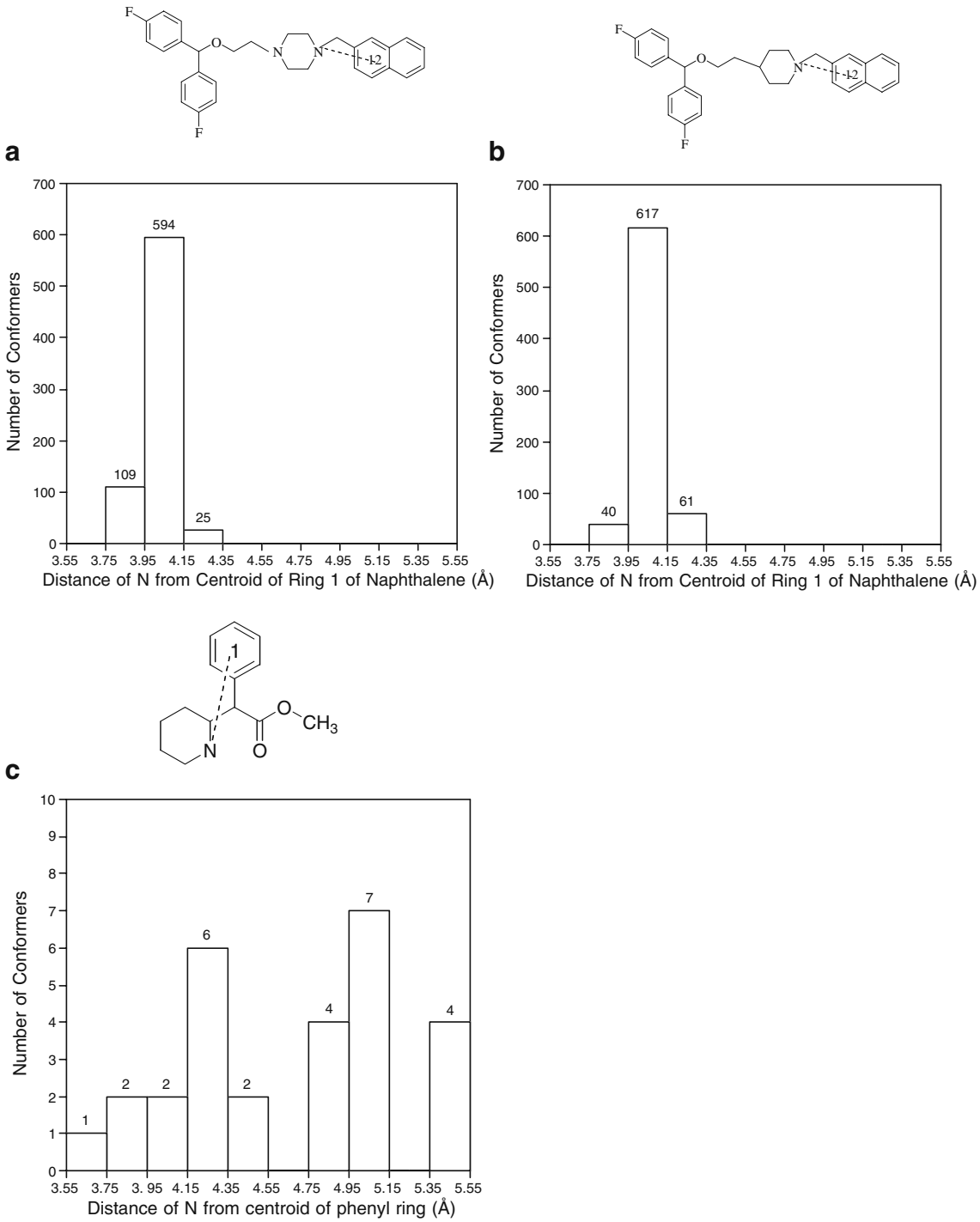

Fig. 12 Number of conformers with a given distance of N from the centroid of the aromatic ring; Tripos force field, vacuum phase. Conformers having distances greater than 3.55 and less than or equal to 3.60 were assigned to the bin labeled 3.55, and so on. **a 2**, **b 3**, **c 4**

subtle differences affect some characteristics of the conformer populations collected during a random search. Ultimately, these differences could affect the results of a 3D-QSAR analysis which depends on the selection of certain representative conformers from a conformer population to act as templates for the analysis. The present work suggests that it is important to check the applicability of the force field for the types of questions one is attempting to answer by computer modeling. In previous work, we used the Tripos vacuum-phase conformer populations of **2** and **3** to select representative conformers [37] as templates for 3D-QSAR analysis of a series of 48 GBR 12909 analogs that differ by changes in the A-side only [5]. This seems an acceptable choice since the differences in the Tripos and

MMFF94 force fields were found to occur only for the nitrogen and oxygen on the B-sides of the analogs.

The results discussed also suggest a possibility that **2**, **3**, and **4** may share a common pharmacophore for DAT binding that involves the aromatic ring and nitrogen. As **2**, **3**, and **4** can orient their common pharmacophore elements in the same way, there is a possibility that the A-sides of the GBR 12909 analogs may attempt to bind to the DAT in a way similar to that of methylphenidate. Of course, the influence of the long B-sides of the GBR 129009 analogs cannot be ruled out, and they may influence this interaction through a range of additional interactions with the DAT protein. Future studies on the more rigid dopamine reuptake inhibitors, similar to the recent study of rigid analogs of methylphenidate [36], will allow a more definitive understanding of the DAT pharmacophore.

Acknowledgments This work was supported in part by grant DA018153 to C.A.V. from the National Institutes of Health (NIH). K.M.G. acknowledges the support of Ruth L. Kirschstein National Research Service Award Individual Predoctoral Fellowship DA015555 from NIH. The authors would like to thank Jeelum Naik, Eun Kim, and Anuj Kumar for assistance with some aspects of the calculations.

References

1. Kuhar MJ, Ritz MC, Boja JW (1991) The dopamine hypothesis of the reinforcing properties of cocaine. Trends Neurosci 14:299–302
2. Prisinzano T, Rice KC, Baumann MH, Rothman RB (2004) Development of neurochemical normalization ("agonist substitution") therapeutics for stimulant abuse: focus on the dopamine uptake inhibitor, GBR 12909. Curr Med Chem Cent Nerv Syst Agents 4:47–59
3. Runyon SP, Carroll FI (2006) Dopamine transporter ligands: recent developments and therapeutic potential. Curr Top Med Chem 6:1825–1843
4. Benedetti P, Mannhold R, Cruciani G, Pastor M (2002) GBR compounds and mepyramines as cocaine abuse therapeutics: chemometric studies on selectivity using grid independent descriptions. J Med Chem 45:1577–1584
5. Gilbert KM, Boos TL, Dersch CM, Greiner E, Jacobson AE, Lewis D, Matecka D, Prisinzano TE, Zhang Y, Rothman RB, Rice KC, Venanzi CA (2007) DAT/SERT selectivity of flexible GBR 12909 analogs modeled using 3D-QSAR methods. Bioorg Med Chem 15:1146–1159
6. Dutta AK, Meltzer PC, Madras BK (1993) Positional importance of the nitrogen atom in novel piperidine analogs of GBR 12909: affinity and selectivity for the dopamine transporter. Med Chem Res 3:209–222
7. Dutta AK, Xu C, Reith ME (1996) Structure–activity relationship studies of novel 4-[2-[bis(4-fluorophenyl)methoxy]ethyl]-1-(3-phenylpropyl)piperidine analogs: synthesis and biological evaluation at the dopamine and serotonin transporter sites. J Med Chem 39:749–756
8. Dutta AK, Reith MEA, Madras BK (2001) Synthesis and preliminary characterization of a high-affinity novel radioligand for the dopamine transporter. Synapse 39:175–181
9. Prisinzano T, Greiner E, Johnson EM II, Dersch CM, Marcus J, Partilla JS, Rothman RB, Jacobson AE, Rice KC (2002) Piperadine analogues of GBR 12909: high affinity ligands for the dopamine transporter. J Med Chem 45:4371–4374
10. Greiner E, Boos TL, Prisinzano TE, De Martino MG, Zeglis B, Dersch CM, Marcus J, Partilla JS, Rothman RB, Jacobson AE, Rice KC (2006) Design and synthesis of promiscuous high-affinity monoamine transporter ligands: unraveling transporter selectivity. J Med Chem 49:1766–1772
11. Zhang S, Fernandez F, Hazeldine S, Deschamps JR, Zhen J, Reith MA, Dutta AK (2006) Further structural exploration of trisubstituted asymmetric pyran derivatives (2*S*,4*R*,5*R*)-2-benzhydryl-5-benzylamino-tetrahydropyran-4-ol and their corresponding disubstituted (3*S*,6*S*)-pyran derivatives: a proposed pharmacophore model for high affinity interaction with the dopamine, serotonin, and norepinephrine transporters. J Med Chem 49:4239–4247
12. Boyd DB, Coner RD (1996) Stochastic approach to force field evaluations: conformational analysis of raloxifene, a potential new therapeutic agent for post-menopausal osteoporosis. J Mol Struct 368:7–15
13. Matecka D, Lewis D, Rothman RB, Dersch CM, Wojnicki FHE, Glowa JR, De Vries AC, Pert A, Rice KC (1997) Heteroaromatic analogs of 1-[2-(diphenylmethoxy)ethyl]- and 1-[2-[bis(4-fluorophenyl)methoxy]ethyl]-4-(3-phenylpropyl)piperazines (GBR 12935 and GBR 12909) as high-affinity dopamine reuptake inhibitors. J Med Chem 40:705–716
14. Clark M, Cramer RD III, Van Opdenbosch N (1989) Validation of the general purpose TRIPOS 5.2 force field. J Comput Chem 10:982–1012
15. Halgren TA (1996) Merck molecular force field. I. Basis, form, scope, parameterization, and performance of MMFF94. J Comput Chem 17:490–519
16. Halgren TA (1996) Merck molecular force field. II. MMFF94 van der Waals and electrostatic parameters for intermolecular interactions. J Comput Chem 17:520–552
17. Halgren TA (1996) Merck molecular force field. III. Molecular geometries and vibrational frequencies for MMFF94. J Comput Chem 17:553–586
18. Halgren TA (1996) Merck molecular force field. IV. Conformational energies and geometries for MMFF94. J Comput Chem 17:587–615
19. Halgren TA, Nachbar R (1996) Merck molecular force field. V. Extension of MMFF94 using experimental data, additional computational data, and empirical rules. J Comput Chem 17:616–641
20. Halgren TA (1999) MMFF VI. MMFF94s option for energy minimization studies. J Comput Chem 20:720–729
21. Halgren TA (1999) MMFF VII. Characterization of MMFF94, MMFF94s, and other widely available force fields for conformational energies and for intermolecular-interaction energies and geometries. J Comput Chem 20:730–748
22. Gundertofte K, Liljefors T, Norrby P, Pettersson I (1996) A comparison of conformational energies calculated by several molecular mechanics methods. J Comput Chem 17:429–449
23. Liljefors T, Gundertofte K, Norby P, Pettersson I (2004) Molecular mechanics and comparison of force fields. In: Bultinck P, Tollenaere JP, Langenaeker W, Winter HD (eds) Computational medicinal chemistry for drug discovery. Marcel Dekker, New York, pp 1–28
24. Banerjee A, Misra M, Pai D, Shih LY, Woodley R, Lu XJ, Srinivasan AR, Olson WK, Davé RN, Venanzi CA (2007) Feature extraction using molecular planes for fuzzy relational clustering of a flexible dopamine reuptake inhibitor. J Chem Inf Model 47:2216–2227
25. Misra M, Banerjee A, Davé RN, Venanzi CA (2005) Novel feature extraction technique for fuzzy relational clustering of a flexible dopamine reuptake inhibitor. J Chem Inf Model 45:610–623

26. Berfield JL, Wang LC, Reith MEA (1999) Which form of dopamine is the substrate for the human dopamine transporter: the cationic or the uncharged species? J Biol Chem 274:4876–4882
27. Xu C, Reith MEA (1996) Modeling the pH dependence of the binding of WIN 35,428 to the dopamine transporter in rat striatal membranes: is the bioactive form positively charged or neutral? J Pharmacol Exp Ther 278:1340–1348
28. Gilbert KA, Skawinski WJ, Misra M, Paris K, Naik N, Deutsch HM, Venanzi CA (2004) Conformational analysis of methylphenidate: comparison of molecular orbital and molecular mechanics methods. J Comput Aided Mol Des 18:719–738
29. Frisch MJ, Trucks GW, Schlegel HB, Scuseria GE, Robb MA, Cheeseman JR, Montgomery Jr. JA, Vreven T, Kudin KN, Burant JC, Millam JM, Iyengar SS, Tomasi J, Barone V, Cossi M, Cammi R, Mennucci B, Pomelli C, Adamo C, Clifford S, Ochterski JW, Ayala PY, Morokuma K, Voth GA, Salvador P, Dannenberg JJ, Zakrzewski VG, Dapprich S, Daniels AD, Strain MC, Farkas O, Malick DK, Rabuck AD, Raghavachari K, Foresman JB, Ortiz JV, Cui Q, Baboul AG, Clifford S, Cioslowski J, Stefanov BB, Liu G, Liashenko A, Piskorz P, Komaromi I, Martin RL, Fox DJ, Keith T, Al-Laham MA, Peng CY, Nanayakkara A, Challacombe M, Gill PMW, Johnson B, Chen W, Wong MW, Gonzalez C, Pople JA (2004) Gaussian 03 C.02.pp. Gaussian Inc., Wallingford
30. Dewar MJS, Zoebisch EG, Healy EE, Stewart JJP (1985) Development and use of quantum mechanical molecular models. 76. AM1: a new general purpose quantum mechanical molecular model. J Am Chem Soc 107:3902–3909
31. Chambers CC, Hawkins GD, Cramer CJ, Truhlar DG (1996) Model for aqueous solvation based on class IV atomic charges and first solvation shell effects. J Phys Chem 100:16385–16398
32. Saunders M (1987) Stochastic exploration of molecular mechanics energy surfaces. Hunting for the global minimum. J Am Chem Soc 109:3150–3152
33. Powell MJD (1977) Restart procedures for the conjugate gradient method. Math Program 12:241–254
34. Fiorentino A, Pandit D, Gilbert KA, Misra M, Dios R, Venanzi CA (2006) Singular valued decomposition of torsional angles of GBR 12909 analogs. J Comput Chem 27:609–620
35. Lowe JP (1968) Barriers to internal rotation about single bonds. Prog Phys Org Chem 6:1–80
36. Kim DI, Deutsch HM, Ye X, Schweri MM (2007) Synthesis and pharmacology of site-specific cocaine abuse treatment agents: restricted rotation analogues of methylphenidate. J Med Chem 50:2718–2731
37. Gilbert KM, Venanzi CA (2006) Hierarchical clustering analysis of flexible GBR 12909 dialkyl piperazine and piperidine analogs. J Comput Aided Mol Des 20:209–225